Remote asymmetric Einstein-Podolsky-Rosen steering of magnons via a single pathway of Bogoliubov dissipation

Deyi Kong,[1] Jun Xu,[1,*] Ya Tian,[1] Fei Wang,[2] and Xiangming Hu[1,†]

[1]*College of Physical Science and Technology, Central China Normal University, Wuhan 430079, People's Republic of China*

[2]*School of Science, Hubei University of Technology, Wuhan 430068, People's Republic of China*

(Received 4 November 2021; accepted 20 January 2022; published 2 February 2022)

We propose a scheme to generate remote asymmetric Einstein-Podolsky-Rosen (EPR) steering of two magnon modes in a hybrid ferromagnet-superconductor system. In our scheme, the indirect coherent coupling between two distant magnons and a Δ-type superconducting atom is established via exchange of virtual photons in two dispersive cavities. As a consequence, the artificial atom acting as a reservoir can produce asymmetrical magnon-magnon steering via a single dissipation channel. Interestingly, we find that the steering directivity is determined by cooling either Bogoliubov mode selectively rather than increasing the extra noise as in conventional schemes. This provides a novel idea to prepare remote EPR steering in solid devices, which may find potential applications in quantum information processing.

DOI: 10.1103/PhysRevResearch.4.013084

I. INTRODUCTION

Magnons, i.e., quanta of collective spin excitations in magnetic materials, have become ideal candidates for studies of macroscopic quantum effects. Thanks to the high spin density of ferromagnetic systems, the magnon mode in a ferromagnetic sphere can strongly couple to the microwave photons via magnetic dipole interaction [1–9]. Many interesting phenomena have been explored in cavity-magnon system, such as magnon dark modes [10], exceptional points [11,12], bistability of cavity-magnon polaritons [13], optical cooling of magnons [14], and nonreciprocity and unidirectional invisibility [15]. Moreover, the magnonic system shows an excellent ability to coherently coupled to diverse quantum systems, including phonons [16,17], optical photons [18–21], and superconducting qubits [22–25]. There are also many novel physical phenomena revealed in hybrid systems based on magnons, ranging from the nonclassical states [26], quantum blockade [27–29], quantum sensing [24,25], and quantum entanglement [30,31]. Notably, due to the unprecedented controllability and scalability of the ferromagnet-superconductor system, it provides a fertile platform to study fundamental quantum physics [27–29,31] and quantum technology [22,24,25].

Einstein-Podolsky-Rosen (EPR) steering, initially introduced by Schrödinger [32] in response to the famous EPR paradox [33], describes the ability of one party to remotely control the other party's states through local measurements. As a strict subset of entanglement and superset of Bell nonlocality [34,35], EPR steering is intrinsically distinct from entanglement and Bell nonlocality due to its asymmetric characteristics. Especially, one-way EPR steering [36,37] shows that the entangled state may be steerable in one direction but not in the other, which provides potential practical applications, e.g., one-sided device-independent quantum cryptography [38–41], quantum secret sharing [42–44], one-way quantum computing [45], no-cloning quantum teleportation [46–48], subchannel discrimination [49], and other related protocols. Recently, genuine photon-magnon-phonon EPR steering [50] and asymmetric steering transfer between photons, magnon, and phonon [51] have been realized in a cavity-magnomechanical system. The EPR entanglement and steering between a macroscopic mechanical oscillator and a distant magnon have also been achieved theoretically [52]. In addition, Zheng *et al*. [53] studied the EPR steering between two macroscopic magnons in a hybrid ferrimagnet-light system and showed strong two-way asymmetric steering between two magnons with equal dissipation. However, it is worthwhile to note that this scheme is confined to the ferrimagnet system, in which the two types of magnons on the two adjacent sublattices are initially entangled. Furthermore, Yang *et al*. [54] implemented stationary one-way quantum steering between two independent magnons, but the involved microwave cavity must be driven by a squeezed vacuum field generated via a flux-driven Josephson parameter amplifier and the magnons are not distant from each other. Therefore, it is worth to further investigate asymmetric EPR steering between two distant magnons by the asymmetry of intrinsic mechanism, rather than through the asymmetry from the external environment.

Long-distance quantum manipulation between macroscopic objects is of crucial importance to various quantum information schemes, especially in the proposals of quantum communication, quantum cryptography, quantum sensing, etc. [55]. Unfortunately, quantum correlation is typically fragile due to the notorious effect of environment-induced decoherence [56]. The search for optimal physical mechanisms that permit robust against decoherence has never ceased.

*junxu@ccnu.edu.cn

†xmhu@ccnu.edu.cn

The dissipation effects were recently explored to prepare the squeezed and entangled states in different schemes [57–64]. There are two main merits for the dissipation mechanisms. First, the squeezing and entanglement by dissipation do not require the preparation of a system in a particular initial state. Second, the squeezing and entanglement can last for an arbitrarily long time and be robust against various random noises. For the four-wave mixing in the two-level atomic system [58,60], a single pathway of Bogoliubov dissipation, in which the only one of a pair of squeeze-transformed modes is mediated into interaction with the atoms and the other is decoupled from the atoms, can lead to the two-mode field squeezing of 50%. To overcome this difficulty, Hu *et al.* [59,62] proposed a two-pathway Bogoliubov dissipation mechanism in a three-level atomic system to enhance the two-mode squeezing to 100%. Although the two-channel dissipation mechanism can effectively improve squeezing and entanglement, it is detrimental to the generation of asymmetric correlation.

In this article, we propose a scheme for establishing a single pathway of Bogoliubov dissipation [61,64] to generate remote asymmetric EPR steering between two magnon modes in a hybrid ferromagnet-superconductor system. Precisely, two ferromagnetic spheres are remotely placed inside two microwave cavities, respectively, and each ferromagnetic sphere is coupled to a cavity mode via linear beam-splitter interaction. Simultaneously, the two microwave cavity fields couple to a Δ-type artificial atom [65] driven by a classical field. When the magnon modes are tuned nearly resonant with the Rabi sidebands of the dressed atom and far-detuned from the microwave cavity fields, the effective coherent coupling between two magnon modes and the superconducting artificial atom can be achieved after adiabatically eliminating the microwave cavity fields. We find that only one of a pair of squeeze-transformed modes on two magnon modes is mediated into interaction with the artificial atom and the other is decoupled. When the coupled Bogoliubov mode is cooled by the artificial atom, the corresponding magnon mode can be steered by the other one, but not vice versa. If the coupled Bogoliubov mode is heated, there will be no steering between the two magnon modes. The direction of the steering is determined by the cooled Bogoliubov mode, which is distinguished from conventional approaches by adding unbalanced losses or noises on the two parties. Compared with other schemes, our scheme has the following striking features: (i) The asymmetric EPR steering does not require the asymmetry from the external environment but utilizes the asymmetry of intrinsic mechanism. (ii) The obtained asymmetric quantum correlations by one-channel Bogoliubov dissipation are immune to environmental decoherence, and do not require the initial preparation of nonclassical states. (iii) The direction of one-way magnon steering can be easily controlled due to the flexible mouldability of the magnons and the superconducting artificial atom.

The remaining part of this article is organized as follows. In Sec. II, we describe the model of the system and obtain the virtual-photon-mediated interaction between the magnons and the dressed atom. In Sec. III, we present the numerical results and then perform the physical analysis and give the corresponding conditions for the quantum correlations of the two magnon modes. The article ends with a conclusion in Sec. IV.

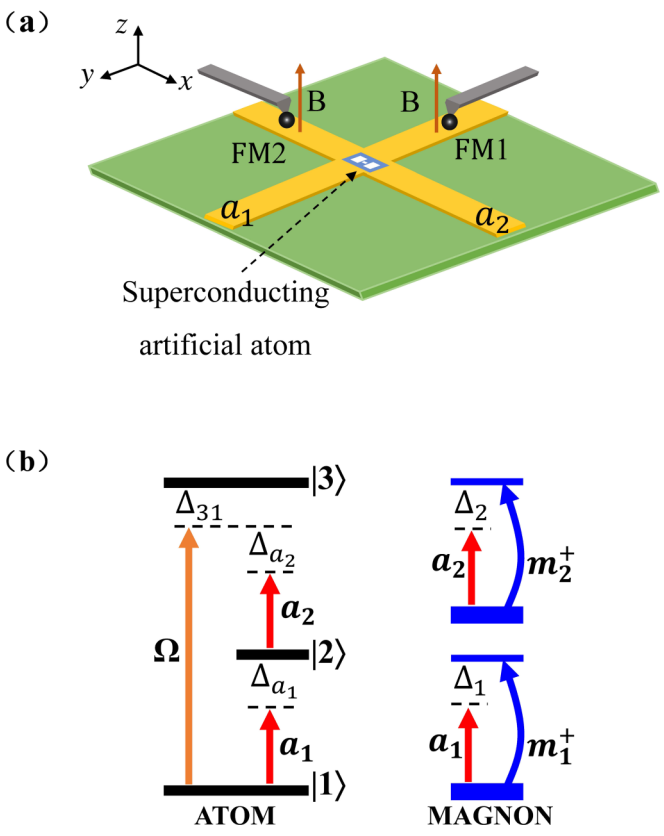

FIG. 1. (a) Sketch of the ferromagnet-superconductor quantum system. The superconducting artificial atom locates at the intersection of two cavities, and the two ferromagnetic (FM) spheres are placed in two different cavity arms, respectively. (b) Interactions of the two cavity fields a_l with the Δ-type artificial atom, which is driven by an external classical field with the Rabi frequency Ω, and the interactions of a_l with the magnon m_l ($l = 1, 2$). The thick and thin blue solid lines represent the ground and excited states of the magnon, and the difference represents the frequency of magnon modes.

II. MODEL AND EQUATIONS

As shown in Fig. 1, we consider a hybrid ferromagnet-superconductor quantum system consisting of a cross-cavity, two ferromagnetic spheres and a Δ-type superconducting artificial atom. The superconducting atom located at the intersection of two cavity arms strongly couples to two microwave cavity modes through the capacitances. Meanwhile, a classical dressing field is applied to the atom. Two ferromagnetic spheres are placed remotely in different cavity arms and strongly coupled to the microwave cavity modes via magnetic-dipole interaction, respectively. The two cavity arms of the cross-cavity are along the x and y directions, respectively. The bias magnetic fields $\mathbf{B}$ are applied locally to the ferromagnetic spheres along the z direction. The two cavity magnetic fields are both perpendicular to the bias magnetic fields, and the two cavity electric fields are parallel to the bias magnetic fields, similar to the experiment scheme as in Ref. [22,66].

In the static limit, the spin-wave modes correspond to magnetostatic modes, where the long-range dipole-dipole interactions between spins are dominant over the short-range exchange interactions [23]. Assuming that the cavity magnetic fields are uniform throughout the ferromagnetic spheres, the magnetic dipole coupling vanishes except for the uniform magnetostatic modes, i.e., the Kittel modes [67]. The Hamiltonian of the hybrid ferromagnet-superconductor system is ($\hbar = 1$)

$$H = H_1 + H_2, \tag{1}$$

where the first part

$$\begin{aligned} H_1 = &\sum_{l=1,2} \omega_{a_l} a_l^\dagger a_l + \sum_{i=2,3} \omega_{i1}\sigma_{ii} \\ &+ \left(g_{a_1} a_1\sigma_{21} + g_{a_2} a_2\sigma_{32} + \Omega\sigma_{31} e^{-i\omega_d t} + \text{H.c}\right), \end{aligned} \tag{2}$$

denotes the interaction of the superconducting artificial atom with the cavity fields and the classical dressing field. a_l and $a_l^\dagger$ are the annihilation and creation operators of the cavity mode at the frequency ω_{a_l}. ω_{i1} is the atomic transition $|i\rangle \to |1\rangle$ frequency. $\sigma_{jk} = |j\rangle\langle k| (j, k = 1, 2, 3)$ are the projection operators for $j = k$ and the spin-flip operators for $j \neq k$. Ω describes the Rabi frequency between artificial atom and the dressing field with the oscillating frequency ω_d. The second term can be expressed as [1]

$$H_2 = \sum_{l=1,2} \left[-g\mu_B B S_l^z + g_{s_l}\left(a_l S_l^- + a_l^\dagger S_l^+\right)\right], \tag{3}$$

which describes the Zeeman effect between the bias magnetic fields and the ferromagnetic spheres, and the magnetic dipole interactions between the cavity fields and the ferromagnetic spheres. g is the g factor, μ_B is the Bohr magneton, and $B = |\mathbf{B}|$ is the amplitude of the bias magnetic fields. $\mathbf{S}_l \equiv (S_l^x, S_l^y, S_l^z)$ stands for the collective spin operator of the two ferromagnetic spheres, g_{s_l} denotes the coupling strength between the macrospin and the cavity mode, and $S_l^\pm \equiv S_l^x \pm iS_l^y$ are the raising and lowering operators of the macrospin, respectively.

The macrospin operators are related to the magnon operators via Holstein-Primakoff transformation [68], $S_l^+ = (\sqrt{2S - m_l^\dagger m_l})m_l$, $S_l^- = m_l^\dagger(\sqrt{2S - m_l^\dagger m_l})$, $S_l^z = S - m_l^\dagger m_l$, where S is the total spin number of the macrospin operator and $m_l^\dagger$ (m_l) is the creation (annihilation) operator of the magnon. For the low-lying excitations with $\langle m_l^\dagger m_l\rangle \ll 2S$, one has $S_l^+ \approx m_l\sqrt{2S}$, and $S_l^- \approx m_l^\dagger\sqrt{2S}$. In this case, the Hamiltonian (3) can be written as

$$H_2 = \sum_{l=1,2} [\omega_{m_l} m_l^\dagger m_l + g_{m_l}(a_l m_l^\dagger + a_l^\dagger m_l)], \tag{4}$$

where $\omega_{m_l} = g\mu_B B$ is the magnon frequency determined by the bias magnetic field, and $g_{m_l} = \sqrt{2S} g_{s_l}$ denotes the magnon-photon coupling strength.

In the rotating frame $H_\text{r} = \omega_d\sigma_{33} + \omega_{21}(\sigma_{22} + a_1^\dagger a_1 + m_1^\dagger m_1) + (\omega_d - \omega_{21})(a_2^\dagger a_2 + m_2^\dagger m_2)$, the total Hamiltonian can be rewritten as

$$H = H_0 + H_\text{d} + H_\text{I}, \tag{5}$$

where the first part

$$H_0 = -\sum_{l=1,2} \left(\Delta_{a_l} a_l^\dagger a_l + \Delta_{m_l} m_l^\dagger m_l\right) \tag{6}$$

is the free part for both the cavity fields and the magnon modes, $\Delta_{a_1,m_1} = \omega_{21} - \omega_{a_1,m_1}$, $\Delta_{a_2,m_2} = \omega_d - \omega_{21} - \omega_{a_2,m_2}$. The second term,

$$H_\text{d} = \Delta_{31}\sigma_{33} + \Omega(\sigma_{13} + \sigma_{31}), \tag{7}$$

denotes the interaction of the superconducting artificial atom with the classical dressing field, where $\Delta_{31} = \omega_{31} - \omega_d$ is the detuning of atomic transition frequency ω_{31} from the dressing field frequency. The last term,

$$H_\text{I} = g_{a_1} a_1\sigma_{21} + g_{a_2} a_2\sigma_{32} + g_{m_1} a_1 m_1^\dagger + g_{m_2} a_2 m_2^\dagger + \text{H.c}, \tag{8}$$

describes the interactions of the cavity fields with both the atom and the magnons through the electric dipole interaction and the magnetic dipole interaction [70]. No direct interaction happens between the superconducting artificial atom and the magnons. Our purpose is to establish the interaction between them by utilizing ancillary dispersive cavities. By transferring the phases of g_{a_l}, g_{m_l} and Ω, respectively, to field operators a_l, the magnon operators m_l, and the atomic spin-flip operators σ_{jk}, we take real values for $g_{a_l} = |g_{a_l}|$, $g_{m_l} = |g_{m_l}|$ and $\Omega = |\Omega|$ ($l = 1, 2$; $j, k = 1, 2, 3$ and $j \neq k$).

The master equation for the density operator ρ of the ferromagnet-superconductor system is written as [70,71]

$$\frac{d}{dt}\rho = -i[H, \rho] + \mathcal{L}_c\rho + \mathcal{L}_m\rho + \mathcal{L}_a\rho. \tag{9}$$

The damping terms in the master equation take the form

$$\begin{aligned} \mathcal{L}_c\rho &= \sum_{l=1,2} \frac{\kappa_{a_l}}{2}(2a_l\rho a_l^\dagger - a_l^\dagger a_l\rho - \rho a_l^\dagger a_l), \\ \mathcal{L}_m\rho &= \sum_{l=1,2} \frac{\kappa_{m_l}}{2}(2m_l\rho m_l^\dagger - m_l^\dagger m_l\rho - \rho m_l^\dagger m_l), \\ \mathcal{L}_a\rho &= \sum_{j\geqslant k} \frac{\gamma_{jk}}{2}(2\sigma_{kj}\rho\sigma_{jk} - \sigma_{jk}\sigma_{kj}\rho - \rho\sigma_{jk}\sigma_{kj}), \end{aligned} \tag{10}$$

where $\mathcal{L}_c\rho$ describes the cavity decays with rates κ_{a_l}, $\mathcal{L}_m\rho$ describes the magnon damping with rates κ_{m_l}, and $\mathcal{L}_a\rho$ describes the artificial atomic decays from states $|j\rangle$ to $|k\rangle$ with rates γ_{jk} ($j, k = 1, 2, 3$) for $j \neq k$, and the dephasing damping for the levels $|j\rangle$ with rates γ_{jj} ($\gamma_{11} = 0$), respectively.

To describe clearly the physical mechanisms and the corresponding conditions for atomic reservoir effects, we transform into the dressed atomic picture. By diagonalizing the Hamiltonian H_d under the conditions of $\Omega \gg \gamma_{jk}, \gamma_{jj}, \kappa_{a_l}, g_{a_l}$, we obtain the dressed states that are expressed in terms of the bare atomic states as [72]

$$\begin{aligned} |+\rangle &= \cos\theta|3\rangle + \sin\theta|1\rangle, \\ |-\rangle &= -\sin\theta|3\rangle + \cos\theta|1\rangle, \end{aligned} \tag{11}$$

where we have defined $\cos\theta = \sqrt{(d + \Delta)/2d}$, $\sin\theta = \sqrt{(d - \Delta)/2d}$, $d = \sqrt{\Delta^2 + 4\Omega^2}$, and $\Delta_{31} = \Delta$. These dressed states $|\pm\rangle$ have their eigenenergies $\lambda_\pm = (\Delta \pm d)/2$, respectively. Now, the Hamiltonian H_d becomes the free form in the dressed-state picture, i.e., $H_\text{d} = \hbar(\lambda_+\sigma_{++} + \lambda_-\sigma_{--})$,

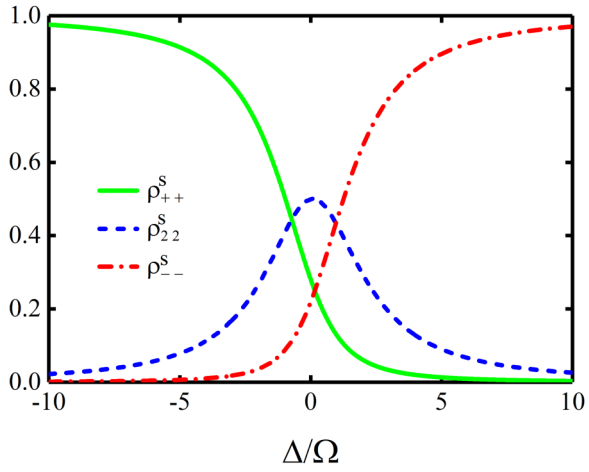

FIG. 2. The atomic dressed state populations as function of the normalized detuning Δ/Ω. We have chosen the parameters similar to those in Ref. [69]: $\gamma_{31} = 2\pi \times 8$MHz, $\gamma_{21} = 2\pi \times 1.5$MHZ, $\gamma_{32} = 2\pi \times 3$MHz, $\gamma_{22} = 2\pi \times 2$MHz, $\gamma_{33} = 2\pi \times 2$MHz.

where we have defined $\sigma_{jk} = |j\rangle\langle k|(j, k = +, -, 2)$ in terms of the dressed atomic states for the projection ($j = k$) and spin-flip ($j \neq k$) operators.

Applying the dressed-state transformation to the artificial atomic relaxation terms and neglecting the weak cavities temporarily, we can obtain the steady dressed-state populations, which are listed in Appendix A. We numerically plot the dressed state populations $\rho^s_{jj}, (j = +, -, 2)$ versus the normalized detuning parameter Δ/Ω in Fig. 2. The steady dressed-state population ρ^s_{++} decreases slowly with an increase of Δ/Ω, then decreases sharply, especially around $\Delta/\Omega = -0.72$, and finally it slowly reduced to almost zero. As the increase of Δ/Ω, ρ^s_{22} first raises slowly to a maximal value at $\Delta/\Omega = 0$ and then decreases gradually. It is also noted that $\rho^s_{++} = \rho^s_{22}$ at the point of $\Delta/\Omega = -0.72$, $\rho^s_{++} > \rho^s_{22}$ for $\Delta/\Omega < -0.72$, and $\rho^s_{++} < \rho^s_{22}$ for $\Delta/\Omega > -0.72$. The variation trends for ρ^s_{--} and ρ^s_{++} are completely opposite, and they reach the same value at $\Delta/\Omega = 0$.

The dressed states are well separated from each other since $d \gg (\gamma's, \kappa's, g's)$. We consider the system operates in the dispersive regime, where cavity fields are far detuned from the dressed atom ($\delta_{1,2} = \Delta_{a_{1,2}} \mp \lambda_+ \gg g_{a_{1,2}}$) and magnon modes ($\Delta_{1,2} = \omega_{m_{1,2}} - \omega_{a_{1,2}} \gg g_{m_{1,2}}$). Simultaneously, we tune the magnon modes nearly resonant with the Rabi sideband ($\Delta_{m_1} \approx -\Delta_{m_2} \approx \lambda_+$). Using the second-order perturbation theory and unitary transformation [73,74] (the detailed derivation is given in Appendix B), we can obtain the effective Hamiltonian

$$H_{\text{eff}} = (g_1 \sin\theta m_1 - g_2 \cos\theta m_2^\dagger)\sigma_{2+} + \text{H.c.}, \tag{12}$$

where we have defined the effective coupling strength $g_l = g_{a_l} g_{m_l}/|\Delta_l|$ $(l = 1, 2)$. In recent experiments, the effective magnon-qubit coupling has already reached $g_{\text{eff}}/2\pi \sim 10$MHz [22]. As for the inevitable decays, the typical value for YIG, ultralow damping of $\kappa_m/2\pi \sim 0.15$ MHz is promising to be realized since the magnon linewidth of $\kappa_m/2\pi \sim 0.6$ MHz with a temperature of 0.1 K$< T <1$ K has been reported [3,26]. For the case of $\Delta_{m_1} \approx -\Delta_{m_2} \approx \lambda_-$, it is treated in the same way, and the dependencies of the quantum correlation on Δ/Ω and g_1/g_2 are symmetrical to the case of $\Delta_{m_1} \approx -\Delta_{m_2} \approx \lambda_+$.

Now it is seen from Hamiltonian (12) that the effective coupling is established between the magnons and the dressed atom. This is based on the simultaneous interactions of the magnons and the atom with the cavity fields. The magnons and atom are pulled into their interaction by adiabatically eliminating the cavity fields, which are far detuned from both the atom and the magnons.

III. ENTANGLEMENT AND STEERING

In this section, we discuss the entanglement and steering of two magnon modes. We give the numerical results, physical analysis, and experimental discussion in the respective three subsections.

A. Numerical results

Following the standard technique [75], we derive the quantum Langevin equations as follows:

$$\begin{aligned} \dot{m}_1 &= -\tilde{\kappa}_{m_1} m_1 - iG_1\sigma_{+2} + F_{m_1}, \\ \dot{m}_2 &= -\tilde{\kappa}_{m_2} m_2 + iG_2\sigma_{2+} + F_{m_2}, \\ \dot{\sigma}_{+2} &= -\Gamma\sigma_{+2} + i\tilde{G}_1 m_1 - i\tilde{G}_2 m_2^\dagger + F_{\sigma_{+2}}, \end{aligned} \tag{13}$$

where we have used $\tilde{\kappa}_{m_l} = \kappa_{m_l}/2$, $G_1 = g_1 \sin\theta$, $G_2 = g_2 \cos\theta$, $\tilde{G}_l = G_l(\rho^s_{22} - \rho^s_{++})$, and $\Gamma = [(\gamma_{31} + \gamma_{32} + \gamma_{33})\cos^2\theta + \gamma_{21} + \gamma_{22}]/2$. The F's are noise terms with zero means and correlations $\langle F_O(t)F_{O'}(t')\rangle = 2D_{OO'}\delta(t - t')$, where the nonzero diffusion coefficients are listed as $2D_{m_l m_l^\dagger} = \kappa_{m_l}$, $2D_{\sigma_{+2}\sigma_{2+}} = 2\Gamma\rho^s_{++}$, $2D_{\sigma_{2+}\sigma_{+2}} = 2\Gamma\rho^s_{22}$ $(l = 1, 2)$. At steady state $\langle m_{1,2}\rangle = \langle\sigma_{+2}\rangle = 0$, then $\delta m_l = m_l$ and $\delta\sigma_{+2} = \sigma_{+2}$. To quantify the entanglement and steering of two magnon modes, we introduce the quadrature components as $\delta X_j = (v_j + v_j^\dagger)/\sqrt{2}$, $\delta P_j = -i(v_j - v_j^\dagger)/\sqrt{2}$, $(v_1 = m_1, v_2 = m_2, v_3 = \sigma_{+2})$, and the noise quadratures F_{X_j} and F_{P_j} are defined in the same way. The quantum Langevin equations of the quadrature fluctuations can be written as the matrix form

$$\dot{u}(t) = -Au(t) + \xi(t), \tag{14}$$

where the column vector for the fluctuation variables is arranged as $u(t) = (\delta X_1, \delta P_1, \delta X_2, \delta P_2, \delta X_3, \delta P_3)^T$, the corresponding noise terms are listed as $\xi(t) = (F_{X_1}, F_{P_1}, F_{X_2}, F_{P_2}, F_{X_3}, F_{P_3})^T$, and the drift matrix reads as

$$A = \begin{pmatrix} \tilde{\kappa}_{m_1} & 0 & 0 & 0 & 0 & -G_1 \\ 0 & \tilde{\kappa}_{m_1} & 0 & 0 & G_1 & 0 \\ 0 & 0 & \tilde{\kappa}_{m_2} & 0 & 0 & -G_2 \\ 0 & 0 & 0 & \tilde{\kappa}_{m_2} & -G_2 & 0 \\ 0 & \tilde{G}_1 & 0 & \tilde{G}_2 & \Gamma & 0 \\ -\tilde{G}_1 & 0 & \tilde{G}_2 & 0 & 0 & \Gamma \end{pmatrix}. \tag{15}$$

The system is stable only if all eigenvalues of the drift matrix A have positive real parts, which can be derived from the Routh-Hurwitz criterion [76]. In the present paper, the

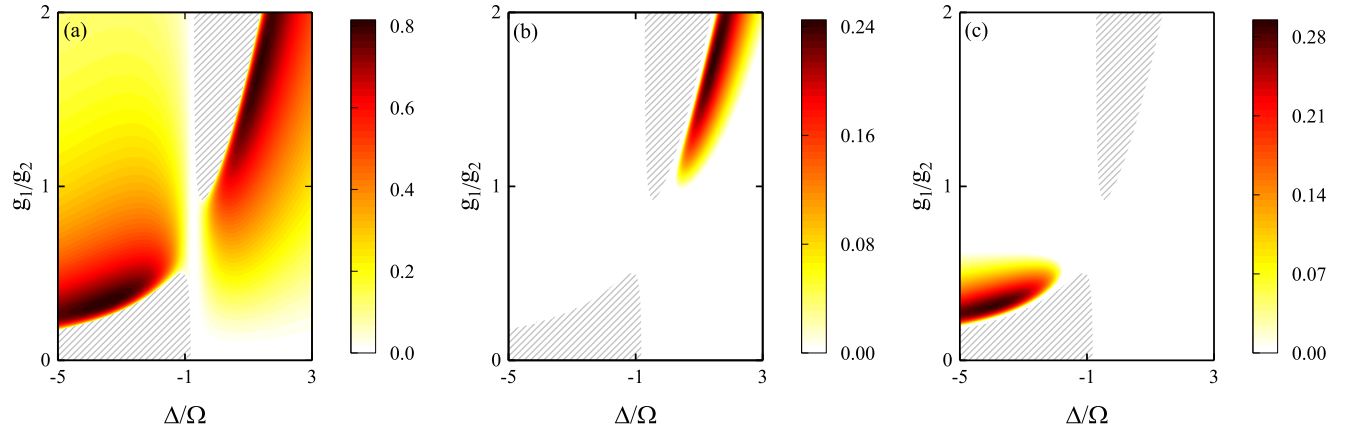

FIG. 3. Density plot of (a) entanglement E_N, (b) steering $\mathcal{G}_{1\to2}$ and (c) steering $\mathcal{G}_{2\to1}$ vs the normalized detuning Δ/Ω and the ratio of coupling strengths g_1/g_2. We have chosen $\kappa_m = 0.1\gamma_{21}$ and $g_2/2\pi = 5$ MHZ. The other parameters are the same as in Fig. 2. The shaded regime shows the unstable region, and the white regimes represent the areas where entanglement and steering do not exist.

chosen parameters satisfy the stability condition. The steady state of the system is a Gaussian state that can be entirely characterized by a 8×8-covariance matrix (CM) C with components $C_{ij}(t,t') = \langle u_i(t)u_j(t') + u_j(t')u_i(t)\rangle/2$, $(i, j = 1, 2, ..., 6)$. The steady-state CM can be achieved by solving the Lyapunov equation [77]

$$AC + CA^T = D, \tag{16}$$

where the diffusion matrix is given by $D = \text{diag}[\tilde{\kappa}_{m_1}, \tilde{\kappa}_{m_1}, \tilde{\kappa}_{m_2}, \tilde{\kappa}_{m_2}, \tilde{\Gamma}, \tilde{\Gamma}]$ with $\tilde{\Gamma} = \Gamma(\rho^s_{22} + \rho^s_{++})$. The diffusion matrix D characterizing the stationary-noise correlations has been defined through $D_{ij}\delta(t-t') = \langle \xi_i(t)\xi_j(t') + \xi_j(t')\xi_i(t)\rangle/2$.

We adopt the logarithmic negativity [78] to quantify the entanglement between the two magnons. This has been proposed as a reliable quantitative estimate of continuous-variable entanglement [79]. The definition of E_N is given by

$$E_N = \max[0, -\ln 2\eta^-], \tag{17}$$

where $\eta^- = \sqrt{\Sigma(V') - [\Sigma(V')^2 - 4\det V']^{1/2}}/\sqrt{2}$ is the smallest symplectic eigenvalue of the partially transposed CM, with $\Sigma(V') \equiv \det V_1 + \det V_2 - 2\det V_{12}$. Here we have considered the reduced CM of two modes of interest

$$V' = \begin{pmatrix} V_1 & V_{12} \\ V_{12}^T & V_2 \end{pmatrix}, \tag{18}$$

where V_1 and V_2 are 2×2 block matrices corresponding to the reduced states of the m_1 and m_2 modes, respectively. It is well known that entanglement exists when $E_N > 0$, and the larger E_N the higher the degree of the entanglement. Moreover, the proposed measurements of the Gaussian quantum steerability in different directions between mode m_1 and mode m_2 are [80]

$$\begin{aligned} \mathcal{G}_{1\to2} &= \max[0, S(2V_1) - S(2V')], \\ \mathcal{G}_{2\to1} &= \max[0, S(2V_2) - S(2V')], \end{aligned} \tag{19}$$

with $S(\sigma) = \ln\det(\sigma)/2$. $\mathcal{G}_{1\to2} > 0$ ($\mathcal{G}_{2\to1} > 0$) demonstrates that the bipartite Gaussian state characterized by the covariance matrix V' is steerable from mode m_1 (m_2) to mode m_2 (m_1) by Gaussian measurements on mode m_1 (m_2). The larger value of $\mathcal{G}$ implies the stronger Gaussian steerability.

For our system, the steady-state values $\langle m^2_{1,2}\rangle = 0$ and $\langle m_1^\dagger m_2\rangle = 0$, such that the conditions to satisfy $E_N > 0$, $\mathcal{G}_{1\to2} > 0$, and $\mathcal{G}_{2\to1} > 0$ can be also expressed in terms of correlation-based inequalities, respectively [81,82],

$$\begin{aligned} |\langle m_1 m_2\rangle| &> \sqrt{\langle m_1^\dagger m_1\rangle\langle m_2^\dagger m_2\rangle}, \\ |\langle m_1 m_2\rangle| &> \sqrt{\langle m_2^\dagger m_2\rangle(\langle m_1^\dagger m_1\rangle + 1/2)}, \\ |\langle m_1 m_2\rangle| &> \sqrt{\langle m_1^\dagger m_1\rangle(\langle m_2^\dagger m_2\rangle + 1/2)}. \end{aligned} \tag{20}$$

From the above equations, we can see that the conditions for generating steering are more demanding than entanglement. The magnon mode with more occupancies is more likely to steer the magnon mode with less occupancies.

The logarithmic negativity E_N and the asymmetric steering quantities $\mathcal{G}_{1\to2}$ and $\mathcal{G}_{2\to1}$ are strongly dependent on two parameters: the normalized detuning Δ/Ω and the coupling strength ratio g_1/g_2, as shown in Figs. 3–5. The physical reason is given in the following subsection. For directly driving the artificial atom, one may adopt the superconducting microwave driving line connected by capacitors. In this case,

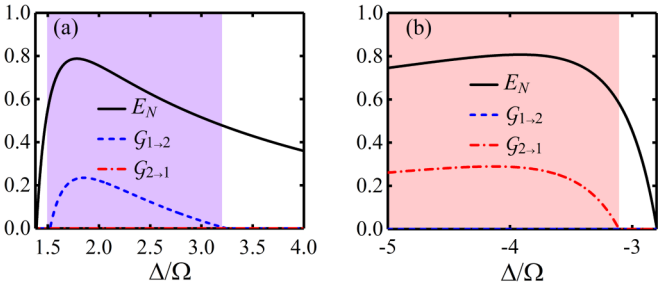

FIG. 4. The entanglement E_N and steering ($\mathcal{G}_{1\to2}$ and $\mathcal{G}_{2\to1}$) vs the normalized detuning Δ/Ω under different ratios of (a) $g_1/g_2 = 2$ and (b) $g_1/g_2 = 0.3$. The other parameters are the same as in Fig. 3. In order to show the steering directivity clearly, we use the purple and pink areas to depict the presence of one-way steering for $m_1 \to m_2$ and $m_2 \to m_1$ respectively, and the white area to describe the presence of no-way steering.

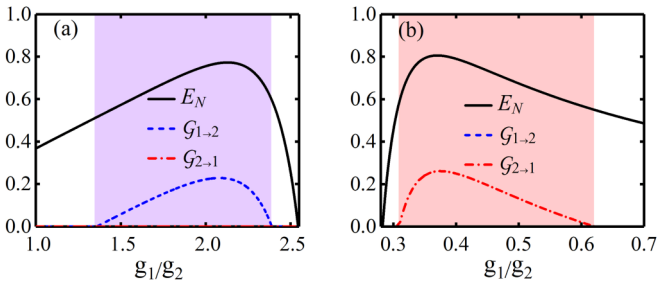

FIG. 5. The entanglement E_N and steering ($\mathcal{G}_{1\to2}$ and $\mathcal{G}_{2\to1}$) vs the ratios of g_1/g_2 under different normalized detuning (a) $\Delta/\Omega = 2$ and (b) $\Delta/\Omega = -3$. The other parameters are the same as in Fig. 3. The color areas represent the same meaning as in Fig. 4.

the normalized detuning Δ/Ω can be changed by adjusting the frequency and intensity of the driving line. Moreover, the flexible modulation of the effective magnon-atom coupling strengths $g_l = g_{a_l} g_{m_l}/\Delta_l$ ($l = 1, 2$) can realize the controllability of the ratio of effective coupling strength without replacing the material. There are three methods to adjust effective coupling strengths: (i) The cavity-atom coupling rates g_{a_l} can be modified by controlling the magnetic flux through the loop of superconducting quantum interference device [69]. (ii) The cavity-magnon coupling rates g_{m_l} can be drastically changed when moving the position of YIG spheres in the cross-shaped cavity [15], due to the inhomogeneity of magnetic field intensity distribution. (iii) The cavity-magnon detuning Δ_l can be tuned by changing the strength of the bias magnetic fields [23].

Plotted in Fig. 3 are the densities of the logarithmic negativity E_N (a), the steering quantities $\mathcal{G}_{1\to2}$ (b) and $\mathcal{G}_{2\to1}$ (c) versus the above two parameters. Here we have chosen the parameters as $\kappa_{m_{1,2}} = \kappa_m = 0.1\gamma_{21}$, $g_2/2\pi = 5$MHZ, the other parameters are the same as in Fig. 2. From Fig. 3, we can see that entanglement exists in most stable parameter regions while steering exists only in a small part of the regime where entanglement exists. This shows that the steering is a strict subset of entanglement. Comparing Fig. 3(b) and Fig. 3(c), it is obvious that the steering is asymmetric, and there is one-way steering in some parameter regions. For example, in the stable regimes of the upper right of Fig. 3(b) and Fig. 3(c), the steering $\mathcal{G}_{1\to2}$ has the nonzero values but the values of $\mathcal{G}_{2\to1}$ is all zero, so there is one-way steering of $m_1 \to m_2$. On the other hand, in the lower left of Fig. 3(b) and Fig. 3(c), one-way steering of $m_2 \to m_1$ exists because only $\mathcal{G}_{2\to1}$ has the nonzero values. This indicates that the implementation and manipulation of one-way EPR steering of magnons can be achieved by adjusting the normalized detuning Δ/Ω and the ratio of coupling strengths g_1/g_2.

Given in Fig. 4 are the logarithmic negativity E_N and the steering quantities $\mathcal{G}_{1\to2}$ and $\mathcal{G}_{2\to1}$ versus the normalized detuning Δ/Ω for different coupling strength ratio g_1/g_2. When $g_1/g_2 = 2$, the E_N first increases and then decreases slowly with an increase of Δ/Ω. The steering $\mathcal{G}_{1\to2}$ has similar variation trends as E_N and reaches the maximum value at the same position. On the contrary, the steering $\mathcal{G}_{2\to1}$ remains zero. When $g_1/g_2 = 0.3$, the steering $\mathcal{G}_{2\to1}$ has nonzero values and has a similar evolutionary trend as E_N, but the steering $\mathcal{G}_{1\to2}$ always remains zero. Similarly, Fig. 5 shows the entanglement and steering versus the ratio g_1/g_2 under the different values of Δ/Ω. For $\Delta/\Omega = 2$, the steering $\mathcal{G}_{2\to1}$ disappears completely, while there is still steering $\mathcal{G}_{1\to2}$. When $\Delta/\Omega = -3$, the steering $\mathcal{G}_{2\to1}$ occurs while the steering $\mathcal{G}_{1\to2}$ vanishes. By analyzing the above numerical results, our scheme shows that the one-way steering with strong entanglement can be achieved by tuning the ratio of g_1/g_2 or the normalized detuning Δ/Ω under appropriate parameter conditions with balanced magnon losses. The most potential application of one-way EPR steering is that it provides security in one-sided device-independent quantum key distribution (QKD) [38–41], where the measurement apparatus of only one party is untrusted.

B. Physical analysis

To understand the essential physics of the phenomena presented in Figs. 4 and 5, we first introduce a pair of Bogoliubov modes as $b_1 = m_1 \cosh r - m_2^\dagger \sinh r$, $b_2 = m_2 \cosh r - m_1^\dagger \sinh r$ [70,71]. Then we substitute modes $b_{1,2}$ for $m_{1,2}$ in Eq. (12), the system Hamiltonian (12) is rewritten as

$$\begin{aligned} H_{\text{eff}} &= g_b(b_1\sigma_{2+} + b_1^\dagger\sigma_{+2}) \quad \text{for} \quad \frac{g_1}{g_2} > \cot\theta, \\ H_{\text{eff}} &= -g_b(b_2\sigma_{+2} + b_2^\dagger\sigma_{2+}) \quad \text{for} \quad \frac{g_1}{g_2} < \cot\theta, \end{aligned} \tag{21}$$

the squeezing parameter r is defined through the hyperbolic tangent function

$$\begin{aligned} \tanh r &= \frac{g_2}{g_1}\cot\theta \quad \text{for} \quad \frac{g_1}{g_2} > \cot\theta, \\ \tanh r &= \frac{g_1}{g_2}\tan\theta \quad \text{for} \quad \frac{g_1}{g_2} < \cot\theta, \end{aligned} \tag{22}$$

where we have defined the corresponding coupling strength $g_b = \sqrt{|g_1^2 \sin^2\theta - g_2^2\cos^2\theta|}$. Depending on the relation between g_1/g_2 and $\cot\theta$ (i.e., Δ/Ω), the interactions between the Bogoliubov modes of magnons and the dressed atom behave differently. That is why we give the dependence on them of the quantities of interest. Obviously, only one Bogoliubov mode b_1 or b_2 is included in Eq. (21). As a result, the one-channel interaction occurs between the transformed modes and the dressed atom. First we consider the ideal case where environmental dissipation can be ignored. For the case of $g_1/g_2 > \cot\theta$, the b_2 mode is decoupled, and the absorption process of b_1 mode is dominant if $\rho_{++}^s > \rho_{22}^s$ and the Bogoliubov mode b_1 is reduced to the vacuum state. In contrast, if $\rho_{++}^s < \rho_{22}^s$, the amplification process of b_1 mode is dominant, and the system is unstable. However, for the case of $g_1/g_2 < \cot\theta$, the b_1 mode is decoupled, and the absorption process of b_2 mode is dominant for $\rho_{++}^s < \rho_{22}^s$ and the b_2 mode evolves to the vacuum state. Especially for the case of the Bogoliubov modes b_1 or b_2 in the vacuum state, the original magnon modes $m_{1,2}$ are in the two-mode squeezed state. As we will see later, the one-channel dissipation established in the present scheme is the key factor to realize the one-way EPR steering.

Next, we include the vacuum environmental dissipation and assume that the atomic variables decay much more rapidly

than the magnons. Following the standard techniques as in [70,71], we derive the master equation of motion for the reduced density operator $\varrho = \mathrm{Tr}_{\mathrm{atom}}\rho$ as

$$\begin{aligned}\dot{\varrho} &= A_1\mathcal{L}_{b_1}\varrho + B_1\mathcal{L}_{b_1^\dagger}\varrho + \mathcal{L}'_m\varrho \quad \text{for} \quad \frac{g_1}{g_2} > \cot\theta,\\ \dot{\varrho} &= A_2\mathcal{L}_{b_2}\varrho + B_2\mathcal{L}_{b_2^\dagger}\varrho + \mathcal{L}'_m\varrho \quad \text{for} \quad \frac{g_1}{g_2} < \cot\theta,\end{aligned} \tag{23}$$

where $\mathcal{L}_O\varrho = (2O\rho O^\dagger - O^\dagger O\rho - \rho O^\dagger O)/2 \quad (O = b_l, b_l^\dagger)$ takes the standard form [70], the absorption (dissipation) rates $A_{1,2}$ and amplification rates $B_{1,2}$ are expressed as $A_1 = B_2 = 2g_b^2\rho^s_{++}/\Gamma$, $A_2 = B_1 = 2g_b^2\rho^s_{22}/\Gamma$. The magnon decay term $\mathcal{L}'_m\varrho$ has the form of

$$\begin{aligned}\mathcal{L}'_m\varrho =& \tilde{\kappa}_m\sum_{l=1,2}[(1+N)(b_l\varrho b_l^\dagger - b_l^\dagger b_l\varrho) + N(b_l^\dagger\varrho b_l - \varrho b_l b_l^\dagger)]\\ &+ 2\tilde{\kappa}_m M(b_1\varrho b_2 + b_2\varrho b_1 - \varrho b_1 b_2 - b_1 b_2\varrho) + \mathrm{H.c.},\end{aligned} \tag{24}$$

where $N = \sinh^2 r$, $M = \sinh r\cosh r$.

The steady-state populations of the modes b_1 and b_2 are obtained from the master equation (23) as

$$\begin{aligned}\langle b_1^\dagger b_1\rangle &= -(\tilde{A}_1 - \tilde{B}_1) + N,\ \langle b_2^\dagger b_2\rangle = N \quad \text{for} \quad \frac{g_1}{g_2} > \cot\theta,\\ \langle b_1^\dagger b_1\rangle &= N,\ \langle b_2^\dagger b_2\rangle = -(\tilde{A}_2 - \tilde{B}_2) + N \quad \text{for} \quad \frac{g_1}{g_2} < \cot\theta,\end{aligned} \tag{25}$$

where the cooling and heating occupancies induced by atomic reservoir are expressed as $\tilde{A}_l = A_l N/\eta_l$, $\tilde{B}_l = B_l(1+N)/\eta_l$, and $\tilde{A}_l - \tilde{B}_l$ represent the net cooling occupancies. We have defined $\eta_l = A_l - B_l + \kappa_m$, and the stability conditions are $\eta_l > 0$ $(l = 1, 2)$. Imagining first that the interaction between the bright Bogoliubov mode and the dressed atom excluded, the modes b_1 and b_2 will have a nonzero intrinsic occupancy N even in the vacuum environment, which implies that vacuum noise driving the magnons acts as effective thermal noise for b_1 and b_2 [83]. In this case, the modes b_1 and b_2 are in a two-mode squeezed vacuum state, which leads to the original magnon modes m_1 and m_2 are in the vacuum state. Obviously, there is no entanglement and steering between two magnons. Now including the effects of the interaction between the bright-mode b_1 and the dressed atom, the dark-mode b_2 is unaffected, whereas the occupancy of the bright-mode b_1 is modified to $\langle b_1^\dagger b_1\rangle = -(\tilde{A}_1 - \tilde{B}_1) + N$ for $g_1/g_2 > \cot\theta$. If $\tilde{A}_1 > \tilde{B}_1$, the cooling (absorption) process of the the bright-mode b_1 is dominant, which means that the one-channel dissipation process is established and it can drive b_1 into the state with little population. As we all know, the linear absorption does not contribute more noise than the vacuum noise to the coupled $m_{1,2}$ modes. Since no spontaneous emission noise enters the $m_{1,2}$ modes, the strong quantum correlation is established through the nonlinearity. So the steady-state asymmetric EPR steering can be achieved via the one-channel dissipation process. On the contrary, for the case of $\tilde{A}_1 < \tilde{B}_1$, the effective gain is larger than absorption, the heating (amplification) process is dominant, and the b_1 evolve into the state with more population. The linear amplification contributes not only linear gain but also extra noise (i.e., spontaneous emission noise) to the $m_{1,2}$ modes. Therefore, the amplifying process contributes to the $m_{1,2}$ modes more noise than the vacuum noise. It is the very spontaneous noise that weakens the quantum correlation between the $m_{1,2}$ modes established through the nonlinearity. Although the quantum correlation generated by amplification process may produce entanglement, but it is too weak to produce steering. Likewise, when we include the effects of the coupling between the bright-mode b_2 and the dressed atom for $g_1/g_2 < \cot\theta$, the dark-mode b_1 is unaffected, whereas the occupancy of the bright-mode b_2 is modified to $\langle b_2^\dagger b_2\rangle = -(\tilde{A}_2 - \tilde{B}_2) + N$, and the physical analysis is similar to the above case. For clearness, we present the above two cases in Tables I, II.

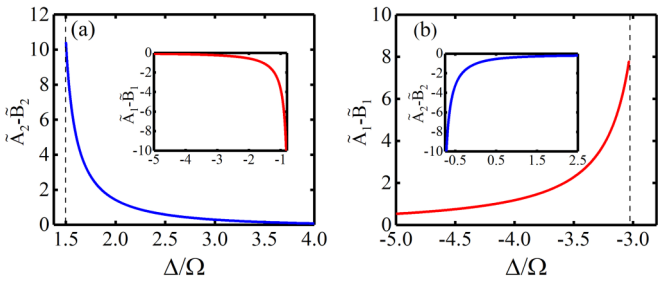

FIG. 6. The net cooling occupancies $\tilde{A}_1 - \tilde{B}_1$ (red line) and $\tilde{A}_2 - \tilde{B}_2$ (blue line) vs the normalized detuning Δ/Ω. When $\tilde{A}_l - \tilde{B}_l > 0$, the cooling (absorption) process is dominant as shown in main maps. On the contrary, for the case of $\tilde{A}_l - \tilde{B}_l < 0$, the heating (amplification) process is dominant as shown in inset maps. The parameters are the same as in Fig. 4.

Figures 6 and 7 displays the net cooling occupancies $\tilde{A}_l - \tilde{B}_l$ versus the normalized detuning Δ/Ω and the radio g_1/g_2, which have chosen the same parameters as in Figs. 4 and 5, respectively. In Fig. 6 it is clear that the atomic reservoir plays different cooling or heating roles for $b_{1,2}$ modes in different regions of Δ/Ω. In the case of $g_1/g_2 = 2$, the b_1 mode is coupled with the atom, and the b_2 mode is decoupled if $\Delta/\Omega < 1.5$. But in this case, the bright-mode b_1 is heated in the stable region, due to $\tilde{A}_1 - \tilde{B}_1 < 0$ from the inset in Fig. 6(a). When $\Delta/\Omega > 1.5$, the b_2 mode is cooled with $\tilde{A}_2 - \tilde{B}_2 > 0$ in the stable region, and the dark-mode b_1 is decoupled, as shown in Fig. 6(a). On the contrary, when $g_1/g_2 = 0.3$, the b_2 mode is decoupled, and the b_1 mode is cooled with $\tilde{A}_1 - \tilde{B}_1 > 0$ for $\Delta/\Omega < -3.03$. The b_1 mode is decoupled and the b_2 mode is heated with $\tilde{A}_2 - \tilde{B}_2 < 0$ for $\Delta/\Omega > -3.03$ in the stable

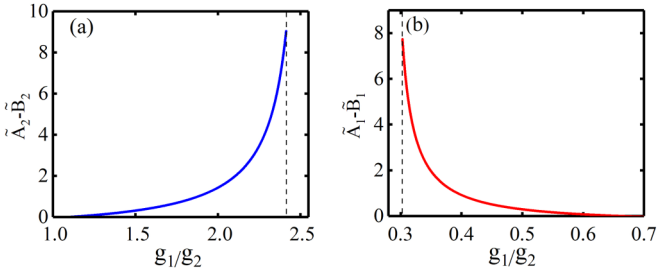

FIG. 7. The net cooling occupancies $\tilde{A}_1 - \tilde{B}_1$ (red line) and $\tilde{A}_2 - \tilde{B}_2$ (blue line) vs the ratio of coupling strengths g_1/g_2. The parameters are the same as in Fig. 5.

TABLE I. One-way EPR steering for $g_1/g_2 > \cot\theta$.

Coupling	Induced occupancies	Cooling	Heating	Populations	One-way steering
b_1	$\tilde{A}_1 > \tilde{B}_1$	Yes	No	$\langle b_1^\dagger b_1\rangle < \langle b_2^\dagger b_2\rangle$	$m_2 \to m_1$
b_1	$\tilde{A}_1 < \tilde{B}_1$	No	Yes	$\langle b_1^\dagger b_1\rangle > \langle b_2^\dagger b_2\rangle$	No

region [Fig. 6(b)]. Similarly, Fig. 7 shows the net cooling occupancy $\tilde{A}_l - \tilde{B}_l$ as a function of g_1/g_2 for fixed Δ/Ω. When $\Delta/\Omega = 2$, the b_2 mode is cooled with $\tilde{A}_2 - \tilde{B}_2 > 0$ in the stable region for $g_1/g_2 < 2.41$. Conversely, for $g_1/g_2 > 2.41$, the b_1 mode is coupled with the dressed atom and heated, and since the system at this time is unstable in most regions, we did not draw the graphs of these intervals [Fig. 7(a)]. However, if $\Delta/\Omega = -3$, as shown in Fig. 7(b), the b_1 mode is cooled due to $\tilde{A}_1 - \tilde{B}_1 > 0$ in the steady-state regime of $g_1/g_2 > 0.31$. The b_2 mode is heated if $g_1/g_2 < 0.31$, and the system is unstable in most regions, so the corresponding graphs are not drawn.

To further analyze the dissipative effect, we will compare the analytical results of the net cooling occupancy [Figs. 6 and 7] and numerical results of entanglement and steering [Figs. 4 and 5]. We can see that the steering exists only in some regions where the net cooling occupancy is greater than zero. This means that the steering exists only possible when dissipation is dominant. Moreover, the behavior of the net cooling occupancy $\tilde{A}_l - \tilde{B}_l$ shown in main maps of Figs. 6 and 7 can also explain the asymmetry of steering, as shown in Figs. 4 and 5. Since the population difference of modes m_1 and m_2 is the same as that of the Bogoliubov modes b_1 and b_2, $\langle m_j^\dagger m_j\rangle - \langle m_k^\dagger m_k\rangle = \langle b_j^\dagger b_j\rangle - \langle b_k^\dagger b_k\rangle = \tilde{A}_k - \tilde{B}_k$, ($j = 2, k = 1$ for $g_1/g_2 > \cot\theta$; $j = 1, k = 2$ for $g_1/g_2 < \cot\theta$). In the case of $g_1/g_2 > \cot\theta$, the fact that the bright-mode b_1 is coupled with the atom reservoir while the dark-mode b_2 is decoupled from them leads to the population $\langle b_1^\dagger b_1\rangle$ always being smaller than $\langle b_2^\dagger b_2\rangle$ when the cooling process is dominant [i.e. $\tilde{A}_1 - \tilde{B}_1 > 0$ as shown in the red lines of Fig. 6(b) and Fig. 7(b)]. Hence, $\langle m_1^\dagger m_1\rangle < \langle m_2^\dagger m_2\rangle$, and the condition for implementing $\mathcal{G}_{2\to1} > 0$ is more accessible to satisfy than the condition for implementing $\mathcal{G}_{1\to2} > 0$, which can be seen from Eq. (20). However, for the heating process is dominant [i.e., $\tilde{A}_1 - \tilde{B}_1 < 0$ as shown in the red line of Fig. 6(a)], $\langle b_1^\dagger b_1\rangle > \langle b_2^\dagger b_2\rangle$, i.e., $\langle m_1^\dagger m_1\rangle > \langle m_2^\dagger m_2\rangle$, which are completely opposite to the situations for realizing one-way steering, and so it is impossible to obtain the steering. For the case of $g_1/g_2 < \cot\theta$, the dark-mode b_1 is decoupled, and the bright-mode b_2 is coupled to the dressed atom. When $\tilde{A}_2 - \tilde{B}_2 > 0$ [blue lines of Fig. 6(a) and Fig. 7(a)], the b_2 mode is cooled and thus $\langle b_2^\dagger b_2\rangle < \langle b_1^\dagger b_1\rangle$, i.e., $\langle m_2^\dagger m_2\rangle < \langle m_1^\dagger m_1\rangle$, which leads to achieve $\mathcal{G}_{1\to2} > 0$ is more accessible than $\mathcal{G}_{2\to1} > 0$ [Figs. 4(a) and 5(a)]. As shown in the blue line of Fig. 6(b), the b_2 mode is heated ($\tilde{A}_2 - \tilde{B}_2 < 0$), and therefore no steering is generated. Theoretically, the larger the net cooling occupancy is, the stronger the quantum correlation will be. However, since the results in Figs. 4 and 5 are under nonadiabatic conditions, there will be some deviation compared with Figs. 6 and 7 in the position of the maximum values. In addition, when the net cooling occupancy is relatively small, the values of $\mathcal{G}_{1\to2}$ and $\mathcal{G}_{2\to1}$ are both equal to zero but E_N is nonzero. That means the quantum correlation between two magnons generated by dissipation effect is too weak to generate steering but enough to generate entanglement in corresponding regions.

C. Experimental implementations

Let us discuss the feasibility of the present scheme. It contains two ferromagnetic spheres, a superconducting artificial atom, and two microwave cavities. In the implementation of experiments, we can use the single crystalline spheres of yttrium iron garnet ($Y_3Fe_5O_{12}$, YIG) as the ferromagnetic samples. Strictly speaking, YIG is a ferrimagnetic material [84,85], and the magnetism is carried by localized Fe moments in 8 tetrahedral (minority) and 12 octahedral (majority) oxygen cages per unit cell, with antiparallel ferrimagnetic states between the two coordinations. The spin wave spectrum of YIG consists of ferromagnetic (acoustic) modes and antiferromagnetic (optical) modes with opposite polarizations. Only the lowest frequency ferromagnetic mode is excited in the low-energy limit [22,86,87]. This enables us to treat YIG as ferromagnet. In addition, YIG exhibits unique features and advantages, including high spin density ($\rho_s = 4.22 \times 10^{27}$ m^{-3}), low damping rate, and large frequency tunability. Experimentally, the strong coupling [2–7] or even ultrastrong coupling [8,9] between the YIG ferromagnetic magnon and microwave photon has been realized. Coherent coupling [22,24] and entanglement [25] between the ferromagnetic magnon in YIG spheres and superconducting qubits are also experimentally implemented. The low-energy YIG spheres used in the above experiments were all treated as ferromagnets. Therefore, it is valid to use YIG spheres in the low-energy limit as the candidates for ferromagnetic spheres in our scheme. Proposed as in Fig. 1(a), the superconducting artificial atom is located in the intersection (near the maximum electric fields) of the cavities, and two distant YIG spheres are mounted in two cavity arms (near the antinode of magnetic field), respectively [88]. In this case, the frequencies of the

TABLE II. One-way EPR steering for $g_1/g_2 < \cot\theta$.

Coupling	Induced occupancies	Cooling	Heating	Populations	One-way steering
b_2	$\tilde{A}_2 > \tilde{B}_2$	Yes	No	$\langle b_1^\dagger b_1\rangle > \langle b_2^\dagger b_2\rangle$	$m_1 \to m_2$
b_2	$\tilde{A}_2 < \tilde{B}_2$	No	Yes	$\langle b_1^\dagger b_1\rangle < \langle b_2^\dagger b_2\rangle$	No

cavity fields must be adjusted flexibly to keep far-detuned from the superconducting artificial atom and magnon modes, and the decay rates of cavities should be large enough to ensure the effective coherent coupling between the dressed atom and magnons after adiabatic elimination of the cavity fields. This can be realized in a planar cross-shaped cavity [66], which formed by using two identical orthogonal half-wavelength microstrip line resonators of sufficient length. As shown in Fig. 1(a), we can use an X-cavity and set locally the bias magnetic fields along the hard magnetization axis (z direction) of YIG spheres. The cavity magnetic fields are respectively with the x and y directions, and the cavity electric fields are along the z direction. In this scheme, we keep the cavity modes empty so that unwanted dephasing caused by photon fluctuations in the the cavities can be avoided. In addition, the impact of the quality factor reduction caused by the damage at the cavity boundaries can be completely ignored since we use cavity fields with large decay rates. Besides, the unnecessary nonlinear effect can be weakened by choosing an appropriate size of YIG spheres.

In the end, the generated magnon entanglement or steering can be detected and verified by measuring the corresponding 4×4 CM, as used in Ref. [89,90]. The states of magnons $m_{1,2}$ can be measured by coupling the magnons to the separate weak microwave probing fields $p_{1,2}$. When the probing fields are resonant with the magnon modes, respectively, the beam-splitter-like interactions $H_{mp}^{l} = g_{p_l}(m_l p_l^{\dagger} + m_l^{\dagger} p_l)$ $(l = 1, 2)$ are thus activated. Therefore, the states of the magnon modes can be transferred onto the probe fields. By homodyning the outputs of the probe fields and measuring the corresponding 4×4 CM, one can verify the entanglement and steering of the magnons.

IV. CONCLUSION

In conclusion, we have proposed a protocol for implementing and manipulating the remote one-way EPR steering of magnons at steady state in the hybrid ferromagnetic-superconducting systems. The two distant magnons are indirectly coupled to a three-level Δ-type superconducting fluxonium qubit via exchange of virtual photons in two dispersive cavities. We find that the one-way steering of magnons can be realized by a single pathway of Bogoliubov dissipation, because the atomic system can act as a reservoir. Instead of introducing asymmetry from the external environment, the steering directivity is determined by cooling either Bogoliubov mode selectively in our scheme, which can be flexibly modulated by adjusting the ratio of the effective magnon-atom coupling strengths g_1/g_2 and the normalized detuning Δ/Ω. Additionally, the asymmetrical magnon-magnon steering by dissipation is robust against the environmental decoherence and do not require the preparation of the system in a particular input state. Furthermore, the remote one-way EPR steering of magnons in massive ferromagnetic spheres belongs to genuinely macroscopic quantum steering and manifests its nonlocal nature. Our paper is thus useful for the investigation of macroscopic quantum effects and quantum information processing.

ACKNOWLEDGMENT

This work is supported by the National Natural Science Foundation of China Grants No. 61875067 and No. 11574179.

APPENDIX A: DRESSED ATOMIC POPULATION

Applying the dressed states transformation to the artificial atomic relaxation terms, we obtain

$$\begin{aligned}\mathcal{L}'_a\rho = &\sum_{m,n=+,-,2} \frac{\Gamma_{mn}}{2}(2\sigma_{nm}\rho\sigma_{nm} - \sigma_{mm}\rho - \rho\sigma_{mm}) \\ &+ \frac{\Gamma_{\mathrm{ph}_1}}{2}(\sigma_{++}\rho\sigma_{--} + \sigma_{--}\rho\sigma_{++}) \\ &+ \frac{\Gamma_{\mathrm{ph}_2}}{2}(2\sigma_p\rho\sigma_p - \sigma_p\sigma_p\rho - \rho\sigma_p\sigma_p),\end{aligned} \tag{A1}$$

wherein $\sigma_p = \sigma_{++} - \sigma_{--}$ and the terms $\Gamma_{mn}(m, n = +, -, 2)$ describe the incoherent population transfer between different dressed states for $m \neq n$ and the phase damping for $m = n$, the terms $\Gamma_{\mathrm{ph}_j}(j = 1, 2)$ are the phase damping terms. The parameters in the above expressions are

$$\begin{aligned}&\Gamma_{+-} = \gamma_{31}\cos^4\theta + \frac{\gamma_{33}}{4}\sin^2 2\theta, \\ &\Gamma_{-+} = \gamma_{31}\sin^4\theta + \frac{\gamma_{33}}{4}\sin^2 2\theta, \\ &\Gamma_{+2} = \gamma_{32}\cos^2\theta,\ \Gamma_{-2} = \gamma_{32}\sin^2\theta, \\ &\Gamma_{2+} = \gamma_{21}\sin^2\theta,\ \Gamma_{2-} = \gamma_{21}\cos^2\theta, \\ &\Gamma_{\mathrm{ph}_1} = \frac{\gamma_{33}}{4}\sin^2 2\theta,\ \Gamma_{\mathrm{ph}_2} = \frac{\gamma_{31}}{4}\sin^2 2\theta, \\ &\Gamma_{++} = \gamma_{33}\cos^4\theta,\ \Gamma_{--} = \gamma_{33}\sin^4\theta,\ \Gamma_{22} = \gamma_{22},\end{aligned} \tag{A2}$$

Neglecting the weak cavity and magnon modes temporarily, we obtain the dynamics equations of the density matrix elements,

$$\begin{aligned}\dot{\rho}_{++} &= -\lambda_{11}\rho_{++} + \lambda_{12}\rho_{--} + \lambda_{13}\rho_{22}, \\ \dot{\rho}_{--} &= \lambda_{21}\rho_{++} - \lambda_{22}\rho_{--} + \lambda_{23}\rho_{22}, \\ \dot{\rho}_{22} &= \lambda_{31}\rho_{++} + \lambda_{32}\rho_{--} - \lambda_{33}\rho_{22},\end{aligned} \tag{A3}$$

where the coefficients in Eq. (A3) are

$$\begin{aligned}&\lambda_{11} = \gamma_{31}\cos^4\theta + \gamma_{32}\cos^2\theta + \frac{\gamma_{33}}{4}\sin^2 2\theta, \\ &\lambda_{12} = \gamma_{31}\sin^4\theta + \frac{\gamma_{33}}{4}\sin^2 2\theta,\ \lambda_{13} = \gamma_{21}\sin^2\theta, \\ &\lambda_{21} = \gamma_{31}\cos^4\theta + \frac{\gamma_{33}}{4}\sin^2 2\theta, \\ &\lambda_{22} = \gamma_{31}\sin^4\theta + \gamma_{32}\sin^2\theta + \frac{\gamma_{33}}{4}\sin^2 2\theta, \\ &\lambda_{23} = \gamma_{21}\cos^2\theta,\ \lambda_{31} = \gamma_{32}\cos^2\theta, \\ &\lambda_{32} = \gamma_{32}\sin^2\theta,\ \lambda_{33} = \gamma_{21}.\end{aligned} \tag{A4}$$

Associating with the closure relation of $\rho_{++} + \rho_{--} + \rho_{22} = 1$, we can obtain the steady-state population ρ_{jj}^{s},

$(j = +, -, 2)$ as

$$\rho^s_{++} = \frac{\lambda_{12}\lambda_{23} + \lambda_{13}\lambda_{22}}{\Lambda},$$
$$\rho^s_{22} = \frac{\lambda_{11}\lambda_{22} - \lambda_{12}\lambda_{21}}{\Lambda}, \tag{A5}$$
$$\rho^s_{--} = \frac{\lambda_{11}\lambda_{23} + \lambda_{13}\lambda_{21}}{\Lambda},$$

where $\Lambda = \lambda_{13}(\lambda_{21} + \lambda_{22}) + \lambda_{12}(\lambda_{23} - \lambda_{21}) + \lambda_{11}(\lambda_{22} + \lambda_{23})$.

APPENDIX B: THE EFFECTIVE HAMILTONIAN

The interaction Hamiltonian $H_{\rm I}$ can be rewritten as $H_{\rm I} = H_{\rm I_1} + H_{\rm I_2}$. The first term

$$H_{\rm I_1} = g_{a_1} a_1 \sigma_{21} + g_{a_2} a_2 \sigma_{32} + \text{H.c.}, \tag{B1}$$

represents the interactions of atom with the cavity fields; and the second term,

$$H_{\rm I_2} = \sum_{l=1,2} g_{m_l} a_l m_l^\dagger + \text{H.c.}, \tag{B2}$$

denotes the interactions of magnons with the cavity fields. In terms of the dressed atomic states, we can use the term $H_{\rm d} - \sum_{l=1,2} \Delta_{a_l} a_l^\dagger a_l$ to make a second rotating transformation. By tuning the cavity fields $\Delta_{a_1} \gg 0$, $\Delta_{a_2} \ll 0$, $(|\lambda_- \mp \Delta_{a_{1,2}}| \gg |\lambda_+ \mp \Delta_{a_{1,2}}|)$ and neglecting the rapidly oscillating terms, the interaction term of the cavity fields and the dressed atom is derived as

$$H'_{\rm I_1} = g_{a_1} \sin\theta a_1 \sigma_{2+} e^{i(\Delta_{a_1} - \lambda_+)t} + g_{a_2} \cos\theta a_2 \sigma_{+2} e^{i(\Delta_{a_2} + \lambda_+)t} + \text{H.c.} \tag{B3}$$

Since the cavity fields are coupled to the atom and the magnons simultaneously, we have to keep the same rotating frames for the cavity fields. That means that we have to return to the original rotating frame. Therefore, the total interaction Hamiltonian of the system is written in the form

$$H'_{\rm I} = (g_{a_1} \sin\theta a_1 + g_{a_2} \cos\theta a_2^\dagger)\sigma_{2+} + \sum_{l=1,2} g_{m_l} a_l m_l^\dagger + \text{H.c.} \tag{B4}$$

Furthermore, we consider that the system operates in the dispersive regime, where the dressed atom-cavity detuning and magnon-cavity detuning are larger than the coupling strength between them i.e., $\delta_{1,2} = \Delta_{a_{1,2}} \mp \lambda_+ \gg g_{a_{1,2}}$, $\Delta_{1,2} = \omega_{m_{1,2}} - \omega_{a_{1,2}} \gg g_{m_{1,2}}$. The effective coupling among the dressed atom and the magnons can be obtained after eliminating the variables of cavity fields by using a unitary transformation $H_{\rm eff} = e^{-\lambda X} H' e^{\lambda X}$, where $H' = H'_0 + H'_{\rm I}$ with the total free Hamiltonian under the dressed state representation $H'_0 = H_0 + H_{\rm d}$. The anti-Hermitian operator X is introduced with the form

$$X = \frac{g_{a_1}}{\delta_1} \sin\theta a_1^\dagger \sigma_{+2} + \frac{g_{a_2}}{\delta_2} \cos\theta a_2^\dagger \sigma_{2+} + \sum_{l=1,2} \frac{g_{m_l}}{\Delta_l} a_l^\dagger m_l - \text{H.c.},$$

which is satisfies as $[H'_0, X] = -H'_{\rm I}$. The λ is introduced to show the orders in the perturbation expansion, and would be set to 1 after the calculations. In terms of the Baker-Campbell-Hausdorff formula, we have

$$\begin{aligned} H_{\rm eff} &= H'_0 + \lambda H'_{\rm I} + \lambda[H'_0, X] + \lambda^2[H'_{\rm I}, X] \\ &\quad + \frac{\lambda^2}{2}[X, [X, H'_0]] + O(\lambda^3) \\ &= H'_0 + \frac{\lambda^2}{2}[H'_{\rm I}, X] + O(\lambda^3). \end{aligned}$$

Tuning the magnon modes of two YIG spheres nearly resonant with the Rabi sidebands of the artificial atom, respectively, i.e., $\Delta_{m_1} \approx -\Delta_{m_2} \approx \lambda_+$, keeping resonant terms only and adiabatically eliminating the empty cavity modes, we can obtain the effective Hamiltonian:

$$\begin{aligned} H_{\rm eff} &= \sum_{j=+,2,-} \nu_j \sigma_{jj} + \sum_{k=1,2} \nu_{m_k} m_k^\dagger m_k \\ &\quad + g_1 \sin\theta (m_1 \sigma_{2+} + m_1^\dagger \sigma_{+2}) \\ &\quad - g_2 \cos\theta (m_2 \sigma_{+2} + m_2^\dagger \sigma_{2+}), \end{aligned}$$

where the effective frequencies are derived as $\nu_+ = \lambda_+ + g_{a_2}^2/\Delta_2$, $\nu_2 = g_{a_1}^2/\Delta_1$, $\nu_- = \lambda_-$, $\nu_{m_l} = -\Delta_{m_l} + g_{m_l}^2/\Delta_l$, $g_l = g_{a_l} g_{m_l}/|\Delta_l|$. Here we should note that $\Delta_l \approx \delta_l (l = 1, 2)$ at the current frequency condition. Applying a new unitary transformation defined by the operator $U = e^{-i(\sum_{j=+,2,-} \nu_j \sigma_{jj} + \sum_{k=1,2} \nu_{m_k} m_k^\dagger m_k)t}$, and assuming $\nu_{m_1} = -\nu_{m_2} = \nu_2 - \nu_+$, we can finally rewrite the effective Hamiltonian as

$$H_{\rm eff} = (g_1 \sin\theta m_1 - g_2 \cos\theta m_2^\dagger)\sigma_{2+} + \text{H.c.} \tag{B5}$$

[1] O. O. Soykal and M. E. Flatté, Size dependence of strong coupling between nanomagnets and photonic cavities, Phys. Rev. B **82**, 104413 (2010); Strong Field Interactions between a Nanomagnet and a Photonic Cavity, Phys. Rev. Lett. **104**, 077202 (2010).

[2] H. Huebl, C. W. Zollitsch, J. Lotze, F. Hocke, M. Greifenstein, A. Marx, R. Gross, and S. T. B. Goennenwein, High Cooperativity in Coupled Microwave Resonator Ferrimagnetic Insulator Hybrids, Phys. Rev. Lett. **111**, 127003 (2013).

[3] Y. Tabuchi, S. Ishino, T. Ishikawa, R. Yamazaki, K. Usami, and Y. Nakamura, Hybridizing Ferromagnetic Magnons and Microwave Photons in the Quantum Limit, Phys. Rev. Lett. **113**, 083603 (2014).

[4] X. Zhang, C.-L. Zou, L. Jiang, and H. X. Tang, Strongly Coupled Magnons and Cavity Microwave Photons, Phys. Rev. Lett. **113**, 156401 (2014).

[5] M. Goryachev, W. G. Farr, D. L. Creedon, Y. Fan, M. Kostylev, and M. E. Tobar, High-Cooperativity Cavity QED with Magnons at Microwave Frequencies, Phys. Rev. Appl. **2**, 054002 (2014).

[6] L. Bai, M. Harder, Y.-P. Chen, X. Fan, J.-Q. Xiao, and C.-M. Hu, Spin Pumping in Electrodynamically Coupled

Magnon-Photon Systems, Phys. Rev. Lett. **114**, 227201 (2015).

[7] D. K. Zhang, X.-M. Wang, T.-F. Li, X.-Q. Luo, W. D. Wu, F. Nori, and J. Q. You, Cavity quantum electrodynamics with ferromagnetic magnons in a small yttrium-iron-garnet sphere, npj Quantum Inf. **1**, 15014 (2015).

[8] J. Bourhill, N. Kostylev, M. Goryachev, D. L. Creedon, and M. E. Tobar, Ultrahigh cooperativity interactions between magnons and resonant photons in a YIG sphere, Phys. Rev. B **93**, 144420 (2016).

[9] N. Kostylev, M. Goryachev, and M. E. Tobar, Superstrong coupling of a microwave cavity to yttrium iron garnet magnons, Appl. Phys. Lett. **108**, 062402 (2016).

[10] X. Zhang, C. L. Zou, N. Zhu, F. Marquardt, L. Jiang, and H. X. Tang, Magnon dark modes and gradient memory, Nat. Commun. **6**, 8914 (2015).

[11] D. Zhang, X.-Q. Luo, Y.-P. Wang, T.-F. Li, and J. Q. You, Observation of the exceptional point in cavity magnon-polaritons, Nat. Commun. **8**, 1368 (2017).

[12] X. Zhang, K. Ding, X. Zhou, J. Xu, and D. Jin, Experimental Observation of an Exceptional Surface in Synthetic Dimensions with Magnon Polaritons, Phys. Rev. Lett. **123**, 237202 (2019).

[13] Y. P. Wang, G. Q. Zhang, D. Zhang, T. F. Li, C. M. Hu, and J. Q. You, Bistability of Cavity Magnon Polaritons, Phys. Rev. Lett. **120**, 057202 (2018).

[14] S. Sharma, Y. M. Blanter, and G. E. W. Bauer, Optical Cooling of Magnons, Phys. Rev. Lett. **121**, 087205 (2018).

[15] Y.-P. Wang, J. W. Rao, Y. Yang, P.-C. Xu, Y. S. Gui, B. M. Yao, J. Q. You, and C.-M. Hu, Nonreciprocity and Unidirectional Invisibility in Cavity Magnonics, Phys. Rev. Lett. **123**, 127202 (2019).

[16] X. Zhang, C.-L. Zou, L. Jiang, and H. X. Tang, Cavity magnomechanics, Sci. Adv. **2**, e1501286 (2016).

[17] J. Li, S.-Y. Zhu, and G. S. Agarwal, Magnon-Photon-Phonon Entanglement in Cavity Magnomechanics, Phys. Rev. Lett. **121**, 203601 (2018).

[18] A. Osada, R. Hisatomi, A. Noguchi, Y. Tabuchi, R. Yamazaki, K. Usami, M. Sadgrove, R. Yalla, M. Nomura, and Y. Nakamura, Cavity Optomagnonics with Spin-Orbit Coupled Photons, Phys. Rev. Lett. **116**, 223601 (2016).

[19] X. Zhang, N. Zhu, C.-L. Zou, and H. X. Tang, Optomagnonic Whispering Gallery Microresonators, Phys. Rev. Lett. **117**, 123605 (2016).

[20] J. A. Haigh, S. Langenfeld, N. J. Lambert, J. J. Baumberg, A. J. Ramsay, A. Nunnenkamp, and A. J. Ferguson, Magneto-optical coupling in whispering-gallery-mode resonators, Phys. Rev. A **92**, 063845 (2015); J. A. Haigh, A. Nunnenkamp, A. J. Ramsay, and A. J. Ferguson, Triple-Resonant Brillouin Light Scattering in Magneto-Optical Cavities, Phys. Rev. Lett. **117**, 133602 (2016).

[21] A. Osada, A. Gloppe, R. Hisatomi, A. Noguchi, R. Yamazaki, M. Nomura, Y. Nakamura, and K. Usami, Brillouin Light Scattering by Magnetic Quasivortices in Cavity Optomagnonics, Phys. Rev. Lett. **120**, 133602 (2018).

[22] Y. Tabuchi, S. Ishino, A. Noguchi, T. Ishikawa, R. Yamazaki, K. Usami, and Y. Nakamura, Quantum magnonics: The magnon meets the superconducting qubit, C. R. Phys. **17**, 729 (2016); Coherent coupling between a ferromagnetic magnon and a superconducting qubit, Science **349**, 405 (2015).

[23] D. Lachance-Quirion, Y. Tabuchi, A. Gloppe, K. Usami, and Y. Nakamura, Hybrid quantum systems based on magnonics, Appl. Phys. Express **12**, 070101 (2019).

[24] D. Lachance-Quirion, Y. Tabuchi, S. Ishino, A. Noguchi, T. Ishikawa, R. Yamazaki, and Y. Nakamura, Resolving quanta of collective spin excitations in a millimeter-sized ferromagnet, Sci. Adv. **3**, e1603150 (2017).

[25] D. Lachance-Quirion, S. P. Wolski, Y. Tabuchi, S. Kono, K. Usami, and Y. Nakamura, Entanglement-based single-shot detection of a single magnon with a superconducting qubit, Science **367**, 425 (2020).

[26] F.-X. Sun, S.-S. Zheng, Y. Xiao, Q. H. Gong, Q. Y. He, and K. Xia, Remote Generation of Magnon Schrödinger Cat State via Magnon-Photon Entanglement, Phys. Rev. Lett. **127**, 087203 (2021).

[27] Z.-X. Liu, H. Xiong, and Y. Wu, Magnon blockade in a hybrid ferromagnet-superconductor quantum system, Phys. Rev. B **100**, 134421 (2019).

[28] J.-K. Xie, S.-L. Ma, and F.-L. Li, Quantum-interference-enhanced magnon blockade in an yttrium-iron-garnet sphere coupled to superconducting circuits, Phys. Rev. A **101**, 042331 (2020).

[29] K. Wu, W.-X. Zhong, G.-L. Cheng, and A.-X. Chen, Phase-controlled multimagnon blockade and magnon-induced tunneling in a hybrid superconducting system, Phys. Rev. A **103**, 052411 (2021).

[30] W.-J. Wu, Y.-P. Wang, J.-Z. Wu, J. Li, and J. Q. You, Remote magnon entanglement between two massive ferrimagnetic spheres via cavity optomagnonics, Phys. Rev. A **104**, 023711 (2021).

[31] D. Y. Kong, X. M. Hu, L. Hu, and J. Xu, Magnon-atom interaction via dispersive cavities: Magnon entanglement, Phys. Rev. B **103**, 224416 (2021).

[32] E. Schrödinger, Discussion of probability relations between separated systems, Proc. Camb. Phil. Soc. **31**, 555 (1935).

[33] A. Einstein, B. Podolsky, and N. Rosen, Can quantum-mechanical description of physical reality be considered complete, Phys. Rev. **47**, 777 (1935).

[34] J. S. Bell, On the Einstein Podolsky Rosen paradox, Physics **1**, 195 (1964).

[35] H. M. Wiseman, S. J. Jones, and A. C. Doherty, Steering, Entanglement, Nonlocality, and the Einstein-Podolsky-Rosen Paradox, Phys. Rev. Lett. **98**, 140402 (2007); S. J. Jones, H. M. Wiseman, and A. C. Doherty, Entanglement, Einstein-Podolsky-Rosen correlations, Bell nonlocality, and steering, Phys. Rev. A **76**, 052116 (2007).

[36] J. Bowles, T. Vértesi, M. T. Quintino, and N. Brunner, One-way Einstein-Podolsky-Rosen Steering, Phys. Rev. Lett. **112**, 200402 (2014).

[37] V. Händchen, T. Eberle, S. Steinlechner, A. Samblowski, T. Franz, R. F. Werner, and R. Schnabel, Observation of one-way Einstein-Podolsky-Rosen steering, Nat. Photonics **6**, 596 (2012).

[38] B. Opanchuk, L. Arnaud, and M. D. Reid, Detecting faked continuous-variable entanglement using one-sided device-independent entanglement witnesses, Phys. Rev. A **89**, 062101 (2014).

[39] C. Branciard, E. G. Cavalcanti, S. P. Walborn, V. Scarani, and H. M. Wiseman, One-sided device-independent quantum key

distribution: Security, feasibility, and the connection with steering, Phys. Rev. A **85**, 010301(R) (2012).

[40] T. Gehring, V. Händchen, J. Duhme, F. Furrer, T. Franz, C. Pacher, R. F. Werner, and R. Schnabel, Implementation of continuous-variable quantum key distribution with composable and one-sided-device-independent security against coherent attacks, Nat. Commun. **6**, 8795 (2015).

[41] N. Walk, S. Hosseni, J. Geng, O. Thearle, J. Y. Haw, S. Armstrong, S. M. Assad, J. Janousek, T. C. Ralph, T. Symul, H. M. Wiseman, and P. K. Lam, Experimental demonstration of Gaussian protocols for one-sided device-independent quantum key distribution, Optica **3**, 634 (2016).

[42] S. Armstrong, M. Wang, R. Y. Teh, Q. H. Gong, Q. Y. He, J. Janousek, H. A. Bachor, M. D. Reid, and P. K. Lam, Multipartite Einstein-Podolsky-Rosen steering and genuine tripartite entanglement with optical networks, Nat. Phys. **11**, 167 (2015).

[43] Y. Xiang, I. Kogias, G. Adesso, and Q. Y. He, Multipartite Gaussian steering: Monogamy constraints and quantum cryptography applications, Phys. Rev. A **95**, 010101(R) (2017).

[44] I. Kogias, Y. Xiang, Q. Y. He, and G. Adesso, Unconditional security of entanglement-based continuous-variable quantum secret sharing, Phys. Rev. A **95**, 012315 (2017).

[45] C. M. Li, K. Chen, Y. N. Chen, Q. Zhang, Y. A. Chen, and J. W. Pan, Genuine High-Order Einstein-Podolsky-Rosen Steering, Phys. Rev. Lett. **115**, 010402 (2015).

[46] M. D. Reid, Signifying quantum benchmarks for qubit teleportation and secure quantum communication using Einstein-Podolsky-Rosen steering inequalities, Phys. Rev. A **88**, 062338 (2013).

[47] Q. Y. He, L. Rosales-Zárate, G. Adesso, and M. D. Reid, Secure Continuous Variable Teleportation and Einstein-Podolsky-Rosen Steering, Phys. Rev. Lett. **115**, 180502 (2015).

[48] C. Y. Chiu, N. Lambert, T. L. Liao, F. Nori, and C. M. Li, No-cloning of quantum steering, npj Quantum Inf. **2**, 16020 (2016).

[49] M. Piani and J. Watrous, Necessary and Sufficient Quantum Information Characterization of Einstein-Podolsky-Rosen Steering, Phys. Rev. Lett. **114**, 060404 (2015).

[50] H. T. Tan, Genuine photon-magnon-phonon Einstein-Podolsky-Rosen steerable nonlocality in a continuously-monitored cavity magnomechanical system, Phys. Rev. Research **1**, 033161 (2019).

[51] Y.-T. Chen, L. Du, Y. Zhang, and J.-H. Wu, Perfect transfer of enhanced entanglement and asymmetric steering in a cavity-magnomechanical system, Phys. Rev. A **103**, 053712 (2021).

[52] H. T. Tan and J. Li, Einstein-Podolsky-Rosen entanglement and asymmetric steering between distant macroscopic mechanical and magnonic systems, Phys. Rev. Research **3**, 013192 (2021).

[53] S. S. Zheng, F. X. Sun, H. Y. Yuan, Z. Ficek, Q. H. Gong, and Q. Y. He, Enhanced entanglement and asymmetric EPR steering between magnons, Sci. China-Phys. Mech. Astron. **64**, 210311 (2020).

[54] Z.-B. Yang, X.-D. Liu, X.-Y. Yin, Y. Ming, H.-Y. Liu, and R.-C. Yang, Controlling Stationary One-Way Quantum Steering in Cavity Magnonics, Phys. Rev. Appl. **15**, 024042 (2021).

[55] M. A. Nielsen and I. L. Chuang, *Quantum Computation and Quantum Information* (Cambridge University Press, Cambridge, 2000).

[56] T. Yu and J. H. Eberly, Sudden death of entanglement, Science **323**, 598 (2009).

[57] H. Tan, G. X. Li, and P. Meystre, Dissipation-driven two-mode mechanical squeezed states in optomechanical systems, Phys. Rev. A **87**, 033829 (2013).

[58] S. Pielawa, G. Morigi, D. Vitali, and L. Davidovich, Generation of Einstein-Podolsky-Rosen-Entangled Radiation through an Atomic Reservoir, Phys. Rev. Lett. **98**, 240401 (2007).

[59] X. M. Hu, Entanglement generation by dissipation in or beyond dark resonances, Phys. Rev. A **92**, 022329 (2015); G. L. Cheng, X. M. Hu, W. X. Zhong, and Q. Li, Two-channel interaction of squeeze-transformed modes with dressed atoms: Entanglement enhancement in four-wave mixing in three-level systems, *ibid.* **78**, 033811 (2008).

[60] X. M. Hu, Q. P. Hu, L. C. Li, C. Huang, and S. Rao, Nonlinearities in reservoir engineering: Enhancing quantum correlations, Phys. Rev. A **96**, 063824 (2017).

[61] F. Wang, W. Nie, and C. H. Oh, Higher-order squeezing and entanglement of harmonic oscillators in superconducting circuits, J. Opt. Soc. Am. B **34**, 130 (2017); F. Wang, W. Nie, X. L. Feng, and C. H. Oh, Steady-state entanglement of harmonic oscillators via dissipation in a single superconducting artificial atom, Phys. Rev. A **94**, 012330 (2016).

[62] W. Wang, X. M. Hu, and J. Xu, Coherent population trapping based atomic reservoir for almost perfect higher-order squeezing, Opt. Express **27**, 30530 (2019).

[63] J. Xu and F. Wang, Perfect higher-order squeezing via strong nonlinearity in microwave-modified electromagnetically induced transparency, Phys. Rev. A **104**, 013706 (2021).

[64] W. X. Zhong, G. L. Cheng, and X. M. Hu, One-way Einstein-Podolsky-Rosen steering via atomic coherence, Opt. Express **25**, 11584 (2017).

[65] Y.-X. Liu, J. Q. You, L. F. Wei, C. P. Sun, and F. Nori, Optical Selection Rules and Phase-Dependent Adiabatic State Control in a Superconducting Quantum Circuit, Phys. Rev. Lett. **95**, 087001 (2005).

[66] J. W. Rao, S. Kaur, B. M. Yao, E. R. J. Edwards, Y. T. Zhao, X. Fan, D. Xue, T. J. Silva, Y. S. Gui, and C. M. Hu, Analogue of dynamic Hall effect in cavity magnon polariton system and coherently controlled logic device, Nat. Commun. **10**, 2934 (2019).

[67] C. Kittel, On the theory of ferromagnetic resonance absorption, Phys. Rev. **73**, 155 (1948).

[68] T. Holstein and H. Primakoff, Field dependence of the intrinsic domain magnetization of a ferromagnet, Phys. Rev. **58**, 1098 (1940).

[69] Z. H. Peng, Y.-X. Liu, J. T. Peltonen, T. Yamamoto, J. S. Tsai, and O. Astafiev, Correlated Emission Lasing in Harmonic Oscillators Coupled via a Single Three-Level Artificial Atom, Phys. Rev. Lett. **115**, 223603 (2015).

[70] M. O. Scully and M. S. Zubairy, *Quantum Optics* (Cambridge University Press, Cambridge, 1997).

[71] D. F. Walls and G. J. Milburn, *Quantum Optics* (Springer, Berlin, 1994).

[72] C. Cohen-Tannoudji, J. Dupont-Roc, and G. Grynberg, *Atom-Photon Interactions* (Wiley, New York, 1992).

[73] M. Alexanian and S. K. Bose, Unitary transformation and the dynamics of a three-level atom interacting with two quantized field modes, Phys. Rev. A **52**, 2218 (1995).

[74] A. Blais, R.-S. Huang, A. Wallraff, S. M. Girvin, and R. J. Schoelkopf, Cavity quantum electrodynamics for

superconducting electrical circuits: An architecture for quantum computation, Phys. Rev. A **69**, 062320 (2004).

[75] C. W. Gardiner and P. Zoller, *Quantum Noise*, 2nd ed. (Springer, Berlin, 2000).

[76] E. X. DeJesus and C. Kaufman, Routh-Hurwitz criterion in the examination of eigenvalues of a system of nonlinear ordinary differential equations, Phys. Rev. A **35**, 5288 (1987).

[77] D. Vitali, S. Gigan, A. Ferreira, H. R. Bohm, P. Tombesi, A. Guerreiro, V. Vedral, A. Zeilinger, and M. Aspelmeyer, Optomechanical Entanglement between a Movable Mirror and a Cavity Field, Phys. Rev. Lett. **98**, 030405 (2007).

[78] G. Vidal and R. F. Werner, Computable measure of entanglement, Phys. Rev. A **65**, 032314 (2002).

[79] G. Adesso, A. Serafini, and F. Illuminati, Extremal entanglement and mixedness in continuous variable systems, Phys. Rev. A **70**, 022318 (2004).

[80] I. Kogias, A. R. Lee, S. Ragy, and G. Adesso, Quantification of Gaussian Quantum Steering, Phys. Rev. Lett. **114**, 060403 (2015).

[81] H. T. Tan, X. C. Zhang, and G. X. Li, Steady-state one-way Einstein-Podolsky-Rosen steering in optomechanical interfaces, Phys. Rev. A **91**, 032121 (2015).

[82] S. S. Zheng, F. X. Sun, Y. J. Lai, Q. H. Gong, and Q. Y. He, Manipulation and enhancement of asymmetric steering via interference effects induced by closed-loop coupling, Phys. Rev. A **99**, 022335 (2019).

[83] Y. D. Wang and A. A. Clerk, Reservoir-Engineered Entanglement in Optomechanical Systems, Phys. Rev. Lett. **110**, 253601 (2013).

[84] Y. Ohnuma, H. Adachi, E. Saitoh, and S. Maekawa, Spin Seebeck effect in antiferromagnets and compensated ferrimagnets, Phys. Rev. B **87**, 014423 (2013).

[85] K. Nakata and S. Takayoshi, Optomagnonic Barnett effect, Phys. Rev. B **102**, 094417 (2020).

[86] J. Barker and G. E. W. Bauer, Thermal Spin Dynamics of Yttrium Iron Garnet, Phys. Rev. Lett. **117**, 217201 (2016).

[87] V. Cherepanov, I. Kolokolov, and V. Lvov, The saga of YIG: Spectra, thermodynamics, interaction and relaxation of magnons in a complex magnet, Phys. Rep. **229**, 81 (1993).

[88] M. Yu, H. Shen, and J. Li, Magnetostrictively Induced Stationary Entanglement between Two Microwave Fields, Phys. Rev. Lett. **124**, 213604 (2020).

[89] T. A. Palomaki, J. D. Teufel, R. W. Simmonds, and K. W. Lehnert, Entangling mechanical motion with microwave fields, Science **342**, 710 (2013).

[90] C. W. Gardiner, Inhibition of Atomic Phase Decays by Squeezed Light: A Direct Effect of Squeezing, Phys. Rev. Lett. **56**, 1917 (1986).